

Electrochemical performances and volume variation of nano-textured silicon thin films as anodes for lithium-ion batteries

This content has been downloaded from IOPscience. Please scroll down to see the full text.

2013 Nanotechnology 24 424011

(<http://iopscience.iop.org/0957-4484/24/42/424011>)

View [the table of contents for this issue](#), or go to the [journal homepage](#) for more

Download details:

IP Address: 159.226.35.87

This content was downloaded on 27/09/2013 at 04:06

Please note that [terms and conditions apply](#).

Electrochemical performances and volume variation of nano-textured silicon thin films as anodes for lithium-ion batteries

Yanhong Wang, Yaoping Liu, Jieyun Zheng, Hao Zheng, Zengxia Mei, Xiaolong Du and Hong Li

Beijing National Laboratory for Condensed Matter Physics, Institute of Physics, Chinese Academy of Sciences, Beijing, 100190, People's Republic of China

E-mail: zxmei@iphy.ac.cn and hli@iphy.ac.cn

Received 31 January 2013, in final form 25 May 2013

Published 25 September 2013

Online at stacks.iop.org/Nano/24/424011

Abstract

Electrochemical behaviors of nano-textured silicon thin film (NTSTF) coated with Al_2O_3 or Cu layers as anodes for lithium-ion batteries have been investigated. The cyclic performance of NTSTF electrodes is superior to dense Si thin films. The NTSTF with a 5 nm thick Cu coating layer shows superior cyclic performance and rate performance to other NTSTF samples. The volume changes of NTSTF electrodes after the first cycle and the tenth cycle have been investigated. This series of electrodes shows an anisotropic volume variation: the height does not change but the diameter does expand. This finding shows the feasibility of dealing with the vertical expansion and contraction of Si-based powder electrodes in Li-ion batteries.

(Some figures may appear in colour only in the online journal)

Introduction

The electrochemical alloying reaction of lithium with silicon at high temperature has been widely studied since the 1970s [1, 2]. Silicon can alloy with lithium to form $\text{Li}_{4.4}\text{Si}$, corresponding to a Li storage capacity of 4200 mAh g^{-1} . In the lithiation process at room temperature, crystalline silicon will convert into amorphous Li_xSi alloy first and then crystallize again at a lithium insertion level above the $\text{Li}_{15}\text{Si}_4$ phase [3–6]. The volume of Si increases linearly by up to 300% after full lithiation [7, 8]. This could lead to the pulverization for micro-sized Si particles or the formation of cracks for dense Si film electrodes [3, 9]. Consequently, the capacity of micro-sized Si powder electrodes drops below 500 mAh g^{-1} after a few cycles [10]. In 1999, the lithium storage behaviors of silicon nanoparticles (SiNPs) and Si nanowires were reported [3, 10]. SiNPs showed a significant advantage in capacity retention compared to micrometer sized silicon particles. However, SiNPs suffered from serious electrochemical agglomeration [3]. In order to solve the volume variation problem, much effort has been expended

on Si-based anodes [11–14]. For practical applications, the volume expansion of the batteries cannot exceed 5–10%, especially in the vertical direction for tablet electronic devices. It has already been noticed that silicon arrays or nanowire electrodes exhibit anisotropic swelling [7, 8, 15, 16]. The volume variation is influenced strongly by the aspect ratio and the substrate. Stand-alone Si nanowires with different crystal orientations show much less expansion in the vertical direction than in the lateral direction [15, 16].

Silicon nanowires [15–20] have been prepared mostly by chemical vapor deposition using silane as the precursor. The fabrication is quite costly and the precursors are difficult to handle. Nano-textured silicon thin film, also named black silicon, has been tested widely in solar cells and photodetectors [21–24]. Large-area nano-textured silicon thin films (NTSTF) can be prepared through a low-cost metal-assisted chemical etching and thermal oxidation method [25]. However, the electrochemical behaviors of NTSTF electrodes have not been studied in Li-ion batteries. In this work, the electrochemical performances and the volume variation of NTSTF electrodes have been investigated.

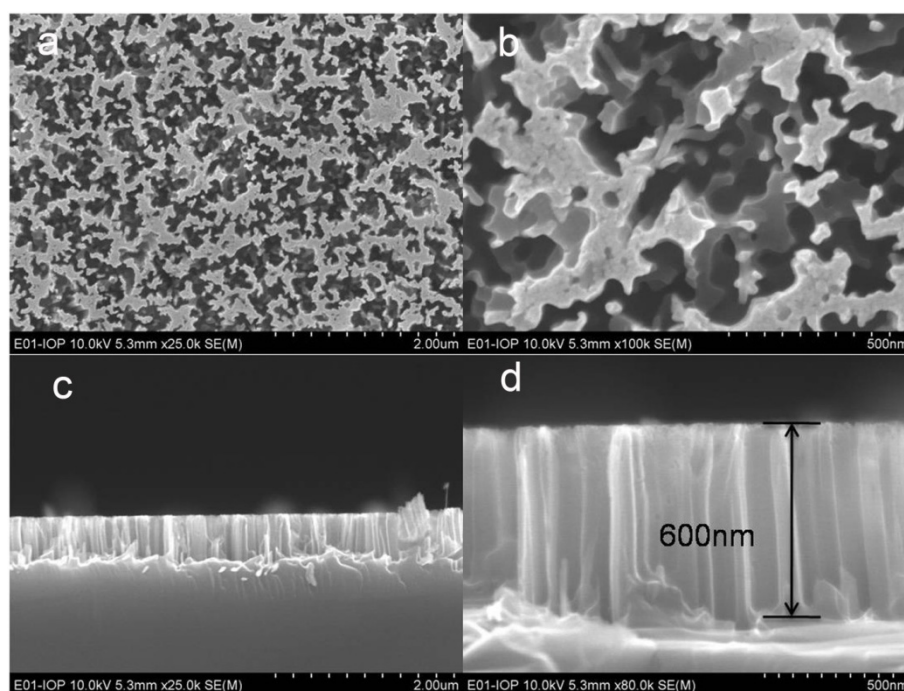


Figure 1. SEM images of top view ((a), (b)) and cross-sectional view ((c), (d)) of pristine nano-textured silicon thin film.

Table 1. Four samples of nano-textured silicon thin films.

Sample name	Thickness of thin film (nm)	Coated film	Thickness of coated layer (nm)	Method of surface coating
A	600	—	0	—
B	600	Al ₂ O ₃	5	Atomic layer deposition
C	600	Cu	5	DC sputtering
D	600	Cu	10	DC sputtering

1. Experimental section

Commercial silicon wafers (Hefei Kejing Materials Technology Co., LTD.) with electrical resistivities of 0.02–0.05 Ω cm were used. The silicon wafers were in the (100) crystallographic orientation and doped as p-type with boron atoms. The NTSTF sheets were prepared using a wet chemical etching method [25]. Then the sheets were cut into 1 \times 1 cm specimens for the experiments. In addition, 5 nm Al₂O₃, 5 nm Cu, 10 nm Cu thin films were coated separately on top of the NTSTF specimens by atomic layer deposition [26] and dc-sputtering methods, respectively. The sample name and the deposition method are listed in the table 1.

A Hitachi 4800 scanning electron microscope (SEM) with an inert atmosphere sample transfer holder was used to observe the surface morphology of pristine and lithiated samples. The crystal structure of the thin films was detected by an X'Pert Pro MPD x-ray diffractometer (XRD) (Philips, Holland) using Cu K α ₁ radiation ($\lambda = 0.15405$ nm), and a Renishaw 1000NR Raman spectrometer using an argon ion laser (wavelength $\lambda = 514$ nm). A high-resolution transmission electron microscope (HRTEM) (Tecnai G2 F20

U-TWIN, FEI, USA) was used to observe the Cu coatings with 5 nm and 10 nm thickness for samples C and D respectively.

A Swagelok-type two-electrode cell was constructed using each of the four samples as the working electrode and a lithium foil as the counter-electrode. The electrolyte was 1M LiPF₆ dissolved in ethylene carbonate (EC) and dimethyl carbonate (DMC) with a volume ratio of 1:1 (Novolyte Technologies Ltd, H₂O < 10 ppm). The cell was assembled in an argon-filled glove box and cycled between 5 mV and 2 V at room temperature using a Land automatic battery tester. The weight of the samples was estimated using a density of 2.33 g cm⁻³. The active material volume is calculated using the 54% cavity volume ratio of the NTSTF in the film layer. The discharge capacity was controlled at 4200 mAh g⁻¹ at each cycle. Therefore, the cell was cycled with a constant discharge capacity of 0.23 mAh. After the initial cycle and the tenth cycle (two states: fully discharged state for full lithiation, fully charged state for delithiation), the electrodes were taken out of the cell and washed by anhydrous DMC to clear away the electrolyte on the surface in the argon-filled glove box and then dried in the vacuum chamber of the glove box. Then the sample was put on a special sample holder for the Hitachi 4800 so it could be transferred into the vacuum chamber of the SEM microscope without exposure to air.

2. Results and discussions

2.1. Microstructure

The morphology of the NTSTF electrode is shown in figure 1. The nanopillars are connected randomly, different from the discrete nanowires [16]. According to the image analysis, the

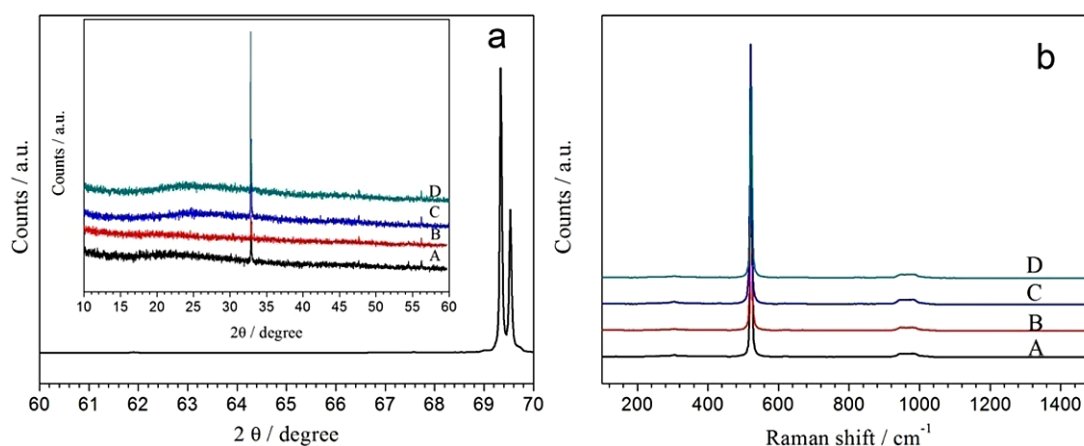


Figure 2. (a) XRD patterns and (b) Raman spectra of the four samples: (A) pristine NTSTF; (B) NTSTF coated with 5 nm Al₂O₃; (C) NTSTF coated with 5 nm Cu; (D) NTSTF coated with 10 nm Cu.

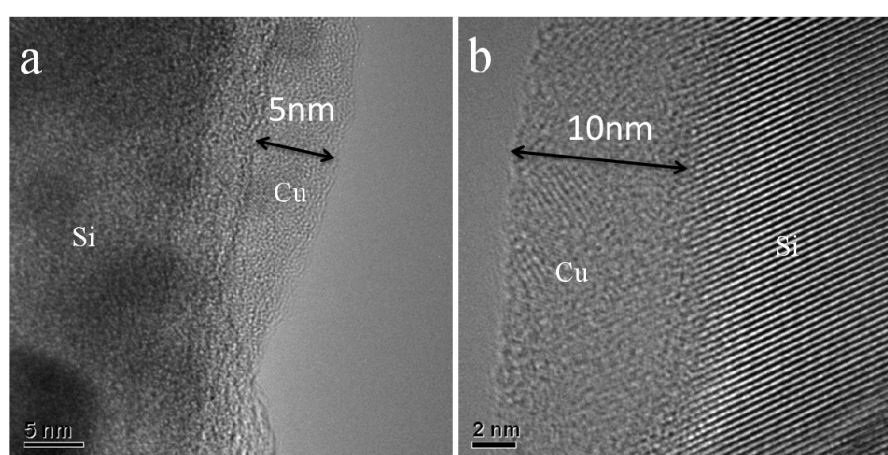


Figure 3. HRTEM images of samples C and D. (a) NTSTF coated with 5 nm Cu; (b) NTSTF coated with 10 nm Cu.

ratio of the cavity area to the total area from the top view is about 54%. There is no crack at the root of the nanopillars from the cross-sectional images shown in figure 1(c). The thickness of the film is about 600 nm, as seen from figure 1(d). After coating with 5 nm Al₂O₃, 5 nm Cu and 10 nm Cu, the morphology of the thin film does not show obvious changes.

The silicon wafer is in the (100) crystallographic orientation. Two XRD peaks around 69° can be observed from figure 2(a). According to the ICDD 00-026-1481 card, the peak at 69.1° is attributed to the (400) plane and the peak at 69.3° is caused by the Cu K α radiation. A very weak peak at 33.2° can also be observed from the inset image of figure 2(a). This belongs to the (200) plane. The crystallinity of the silicon crystal is also shown in the Raman spectra in figure 2(b). The Raman vibration mode at 520 cm⁻¹ corresponding to the TO mode is very sharp for each of the four samples, indicating their high crystallinity.

For sample B, 50 cycles of Al₂O₃ ALD were performed on the surface of the NTSTF sheet using trimethyl aluminum (TMA) and H₂O as precursors at 250 °C, and the coating thickness of Al₂O₃ was about 5 nm. The ALD coating layer covers the whole surface uniformly in all cases. In the case of the 5 nm and 10 nm Cu coatings, as shown in the TEM

images in figures 3(a) and (b), a polycrystalline Cu layer is coated on the ‘sidewall’ of the Si pillar. Since the TEM images represent only a few silicon nanopillars scratched from the textured silicon thin film, we are not sure whether the Cu coating can cover the sidewalls of all the silicon nanopillars in the NTSTF electrode.

2.2. Electrochemical performance

Figure 4 shows the charge and discharge curves of the four samples for the first 10 cycles. The voltage profiles are typical for a-Si electrodes. The initial Coulombic efficiency of the four samples is 88%, 60.4%, 84.5% and 85.8%, respectively. Since the discharging capacity is kept the same, the low initial Coulombic efficiency means that a significant ratio of inserted lithium is trapped by the sample. This could be related to the irreversible consumption to form the surface films, trapping by the internal defects or the loss of electronic contact for some lithiated parts. This will be clarified later. According to figure 4, neither the Al₂O₃ layer nor the Cu layer hinder the insertion and extraction of lithium.

Figure 5 shows the cyclic performance and the rate performance. It can be seen that the pristine NTSTF electrode

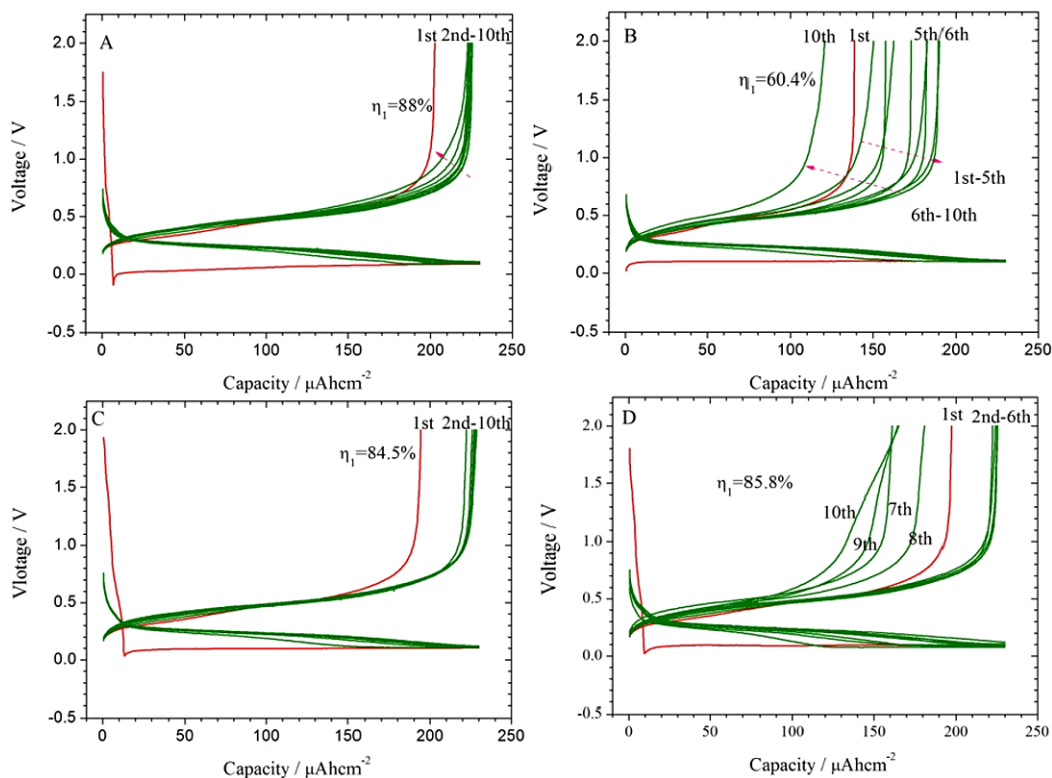


Figure 4. Discharge and charge performance of the four samples in the first ten cycles: (A) pristine NTSTF; (B) NTSTF coated with 5 nm Al_2O_3 ; (C) NTSTF coated with 5 nm Cu; (D) NTSTF coated with 10 nm Cu.

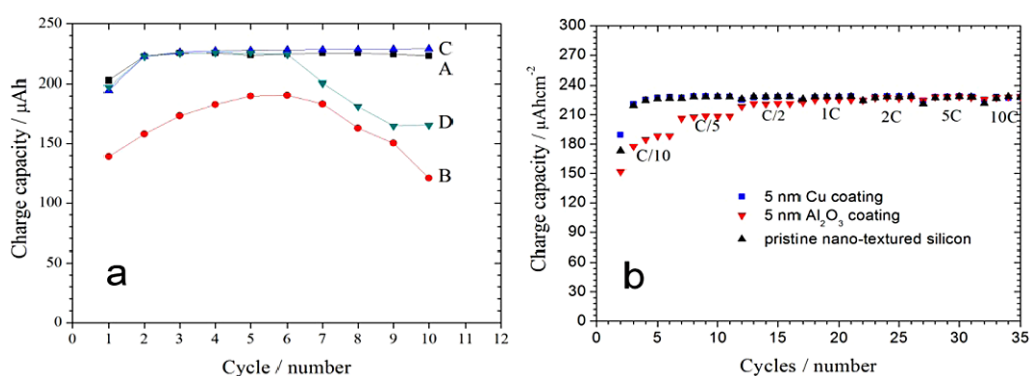


Figure 5. (a) Cyclic performance and (b) rate performance of the four samples in the first 10 cycles: (A) pristine NTSTF; (B) NTSTF coated with 5 nm Al_2O_3 ; (C) NTSTF coated with 5 nm Cu; (D) NTSTF coated with 10 nm Cu.

and the 5 nm Cu-coated NTSTF sample show a higher capacity and better cyclic performance and rate performance. The 5 nm Al_2O_3 coated NTSTF shows a lower capacity and a poor cyclic performance. Our previous investigation indicated that Si microdisks coated by 2 nm Al_2O_3 can show a superior electrochemical performance, while 4 nm Al_2O_3 coated Si microdisks did not show activity for lithium storage [26]. In this case it is probable that the 5 nm Al_2O_3 coating could not completely coat the surface of the NTSTF due to its irregularity. Still, the 5 nm Al_2O_3 coating shows a negative effect. It is noticed that the capacity of the 5 nm Al_2O_3 coated NTSTF increases gradually for the first six cycles and then decreases. This indicates an activation process and will be explained later.

The polarization of the electrodes is analyzed with dQ/dV curves, as shown in figure 6. The electrode area, current density and other measurement conditions are the same for all samples. Therefore, the voltage of the electrodes can be used to compare the polarization. The lithium insertion at the first cycle shows a different voltage profile due to the high initial polarization. It is not included in the dQ/dV curves. In the dQ/dV curves shown in figure 6, the peaks around 0.31 V and 0.49 V during oxidation (charging) are assigned as O1 and O2 peaks. The peak around 0.23 V during reduction (discharging) is assigned as the R1 peak. Another reduction peak around 0.0–0.1 V is difficult to assign. It should be mentioned that the appearance of two peaks indicates a two-step phase transition procedure, which has

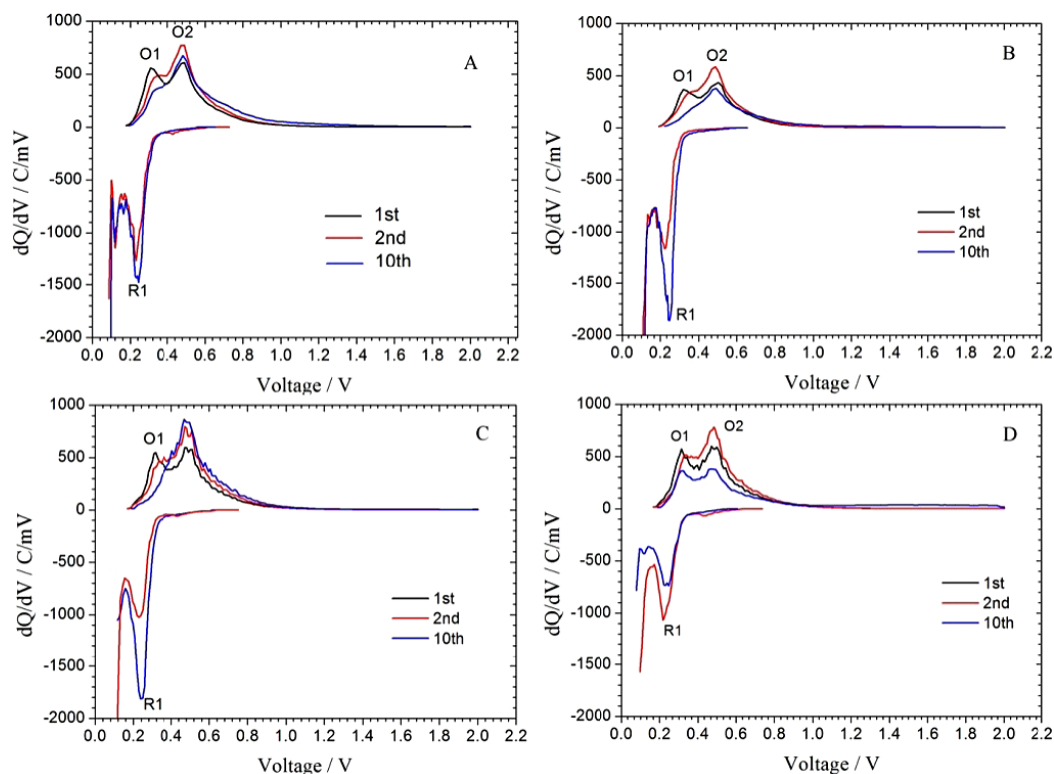


Figure 6. The dQ/dV curves redrawn from the galvanostatic discharging/charging curves in figure 4. (A) pristine NTSTF; (B) NTSTF coated with 5 nm Al_2O_3 ; (C) NTSTF coated with 5 nm Cu; (D) NTSTF coated with 10 nm Cu.

Table 2. Voltage and polarization information of the NTSTF electrodes from the dQ/dV curves.

Sample	O1 (1st/2nd/10th) (V)	O2 (1st/2nd/10th) (V)	R1 (2nd/10th) (V)	Δ (O1 – R1) (2nd/10th) (V)
A	0.312/0.335/0.346	0.484/0.484/0.484	0.229/0.239	0.255/0.245
B	0.320/0.350/0.380	0.510/0.484/0.484	0.224/0.247	0.260/0.237
C	0.312/0.342/0.378	0.490/0.485/0.478	0.232/0.242	0.253/0.236
D	0.314/0.333/0.317	0.487/0.482/0.478	0.216/0.235	0.262/0.243

been noticed previously [9, 27]. This could be related to a two-step reaction from a-Si to a- $\text{Li}_{2.5}\text{Si}$ and from a- $\text{Li}_{2.5}\text{Si}$ to a- $\text{Li}_{3.75}\text{Si}$ [27]. The voltage information is listed in table 2. It can be seen that the initial oxidation voltages of the 5 nm Al_2O_3 coated NTSTF electrode are higher than all the other samples. Also, Cu-coated NTSTF thin films show a similar polarization to uncoated NTSTF. Since the polarization of each electrode shows no significant difference from the dQ/dV curve, it implies that other factors have an impact on the electrochemical performance.

2.3. Volume variation

Since it is hard to identify the total volume variation based on TEM investigations on a few scratched Si nanopillars due to their ill-defined morphology, we felt that it would be more accurate to get the total volume variation by calculating the porosity variation, which could be obtained from SEM investigations.

The top view SEM images of the four types of NTSTF electrode after the first cycle and the tenth cycle are shown in

figure 7. Except for the 5 nm Al_2O_3 coated NTSTF electrode, the samples show a significant change in the porosity ratio after lithium insertion and extraction. For sample B with the 5 nm Al_2O_3 coating, the SEM images do not change from the top view. This means that little lithium is inserted into the nanopillars in the first cycle. For sample C, in figure 7(i), the porosity is decreased significantly. The nanopillar structure seems to disappear for the 5 nm Cu-coated NTSTF electrode after ten cycles. The merged nanopillars do not separate back to the initial structure after lithium extraction. This room-temperature irreversible electrochemical agglomeration phenomenon is similar to our previous investigations on silicon nanoparticles [3] and Si microdisk electrodes [8]. Nano-textured silicon thin films can also be regarded as the model material for porous silicon. Our results indicate clearly that the initial porous structure could vary significantly after repeated lithiation and delithiation.

A rough statistic analysis on the ratio of the cavity area to the total surface area from the top view is performed by analyzing the SEM images. The results are listed in table 3. It can be seen that the cavity ratios for the 5 nm Cu-coated NTSTF and uncoated NTSTF decrease from an initial 54% to

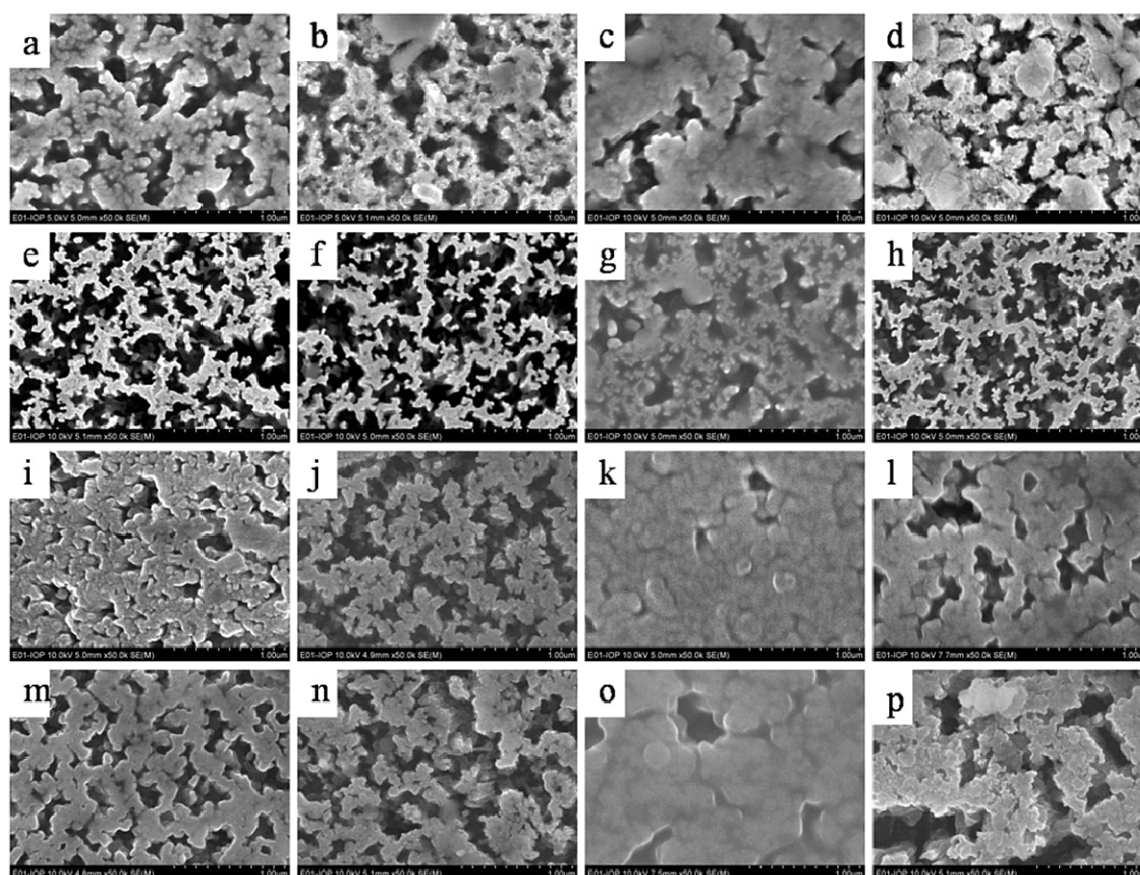


Figure 7. Top view SEM images after various numbers of cycles: Sample A: (a) 1st insertion, (b) 1st extraction, (c) 10th insertion, (d) 10th extraction; Sample B: (e) 1st insertion, (f) 1st extraction, (g) 10th insertion, (h) 10th extraction; Sample C: (i) 1st insertion, (j) 1st extraction, (k) 10th insertion, (l) 10th extraction. Sample D: (m) 1st insertion, (n) 1st extraction, (o) 10th insertion, (p) 10th extraction. The scale bar in each figure is 1 μm .

Table 3. Cavity ratio on top surface of the NTSTF electrodes before and after lithiation.

Sample State	(A) NTSTF	(B) 5 nm Al_2O_3	(C) 5 nm Cu	(D) 10 nm Cu
Origin	54%	54%	54%	54%
First insertion	28%	43%	6%	37%
First extraction	28%	42%	39%	19%
Tenth insertion	6%	22%	3%	9%
Tenth extraction	25%	38%	15%	12%

3% and 6% respectively after the tenth lithium insertion. This indicates the obvious expansion of the nanopillar. The sample of 5 nm Al_2O_3 coated NTSTF shows a large cavity ratio of 22% after the tenth lithium insertion. This indicates that the expansion of nanopillar in sample B is the least significant.

The SEM images from the top view at low magnification are shown in figure 8. Many cracks can be seen clearly for all the samples. The Cu coating seems to be effective in decreasing the crack width, similar to the function of Ti nanograins dispersed into a-Si matrix [9]. From these images, it can be seen that even for the nano-textured Si electrode with a high ratio of porosity, cracking is unavoidable due to the electrochemical agglomeration after the first cycle. Note that the porous structure could accommodate a large volume

variation, but could not maintain a stable microstructure during repeated lithiation and delithiation.

The SEM images of the cross-sectional view of all samples are shown in figure 9. Nearly all the nanopillars are connected to the Si substrate after cycling, without obvious breaking or peeling off. This could be an advantage of this type of material. The height change is not very significant. The data is shown in figure 10(a). With the height and porosity variation data, the volume variation $\Delta V\%$ can be estimated from the equation:

$$\Delta V\% = S_i(1 - \theta_i) * H_i/S_0(1 - \theta_0) * H_0 - 1. \quad (1)$$

Here S_i and S_0 are the surface area of the electrode at the other state and the initial state, H_i and H_0 are the height of the electrode at the other state and the initial state, θ_i and θ_0 are the cavity ratio of the electrode at the other state and the initial state. In this study, $S_i = S_0$.

It can be seen in figure 10(a) that after the first lithium insertion, the height of the nanopillars for sample C does not change, for sample D it changes slightly and for sample B it is increased; while the total volume variation is not in that case. It is already known that a 2 nm Al_2O_3 coating does not influence the electrochemical lithium insertion and extraction, as reported by us previously [26]. It seems that a 5 nm Al_2O_3 coating blocks the insertion of lithium into the Si nanopillars.

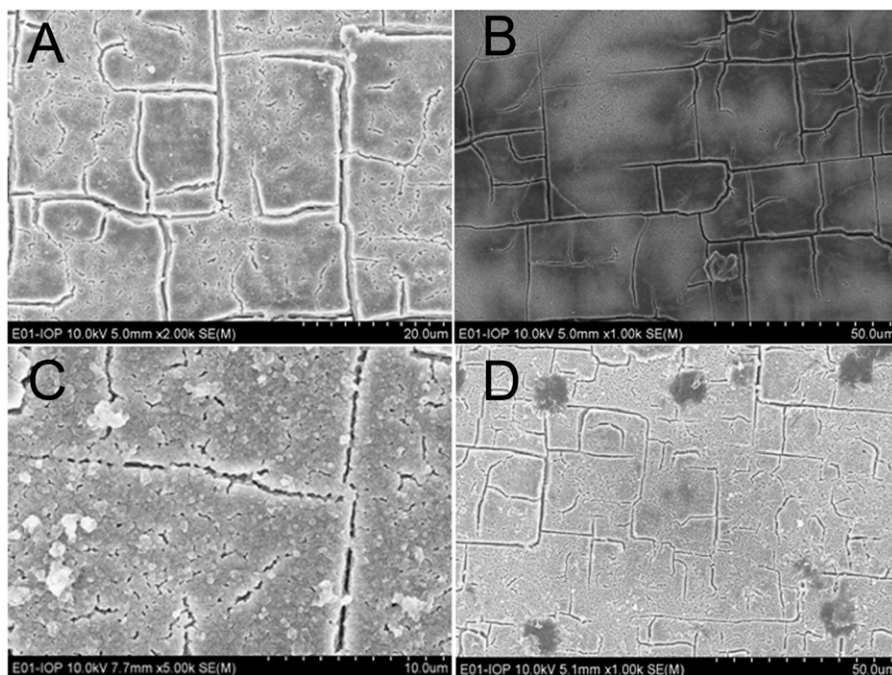


Figure 8. Top view images of the NTSTF electrodes after the tenth cycle at the lithium extraction state at low magnification, (A) pristine NTSTF; (B) NTSTF coated with 5 nm Al_2O_3 ; (C) NTSTF coated with 5 nm Cu; (D) NTSTF coated with 10 nm Cu.

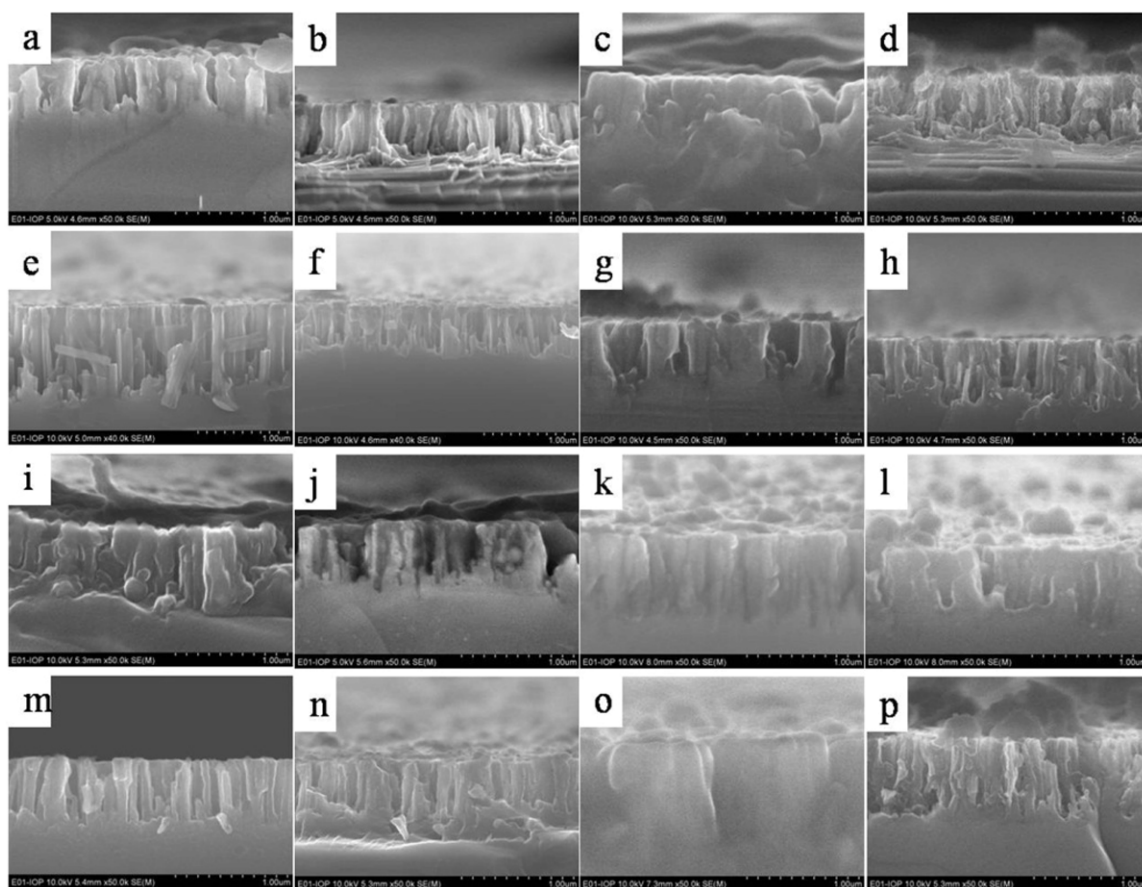


Figure 9. Cross-section view SEM images after various numbers of cycles. Sample A: (a): 1st insertion, (b) 1st extraction, (c) 10th insertion, (d) 10th extraction. Sample B: (e) 1st insertion, (f) 1st extraction, (g) 10th insertion, (h) 10th extraction. Sample C: (i) 1st insertion, (j) 1st extraction, (k) 10th insertion, (l) 10th extraction. Sample D: (m) 1st insertion, (n) 1st extraction, (o) 10th insertion, (p) 10th extraction. The scale bar in each figure is 1 μm .

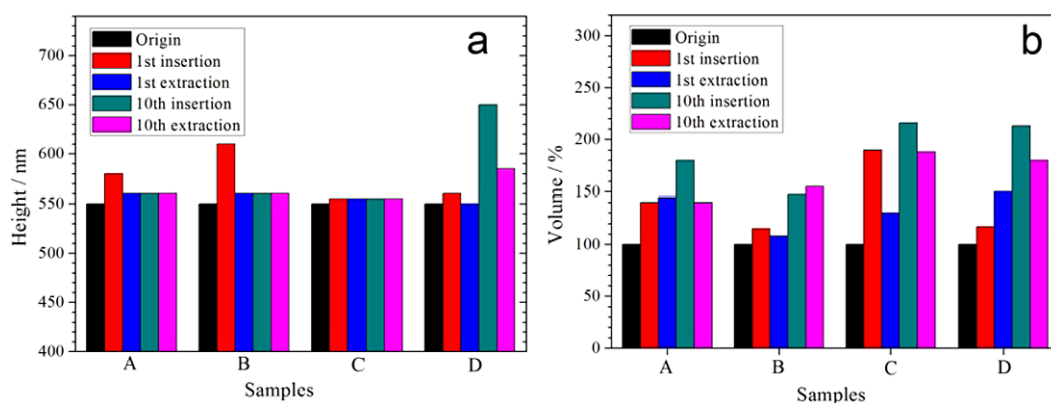


Figure 10. (a) Height change and (b) volume change of the four samples in different states and cycles: (A) pristine NTSTF; (B) NTSTF coated with 5 nm Al_2O_3 ; (C) NTSTF coated with 5 nm Cu; (D) NTSTF coated with 10 nm Cu.

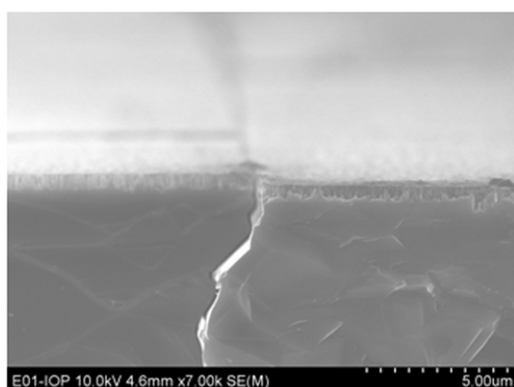


Figure 11. The cross-sectional image of the NTSTF coated with 5 nm Al_2O_3 after the first lithium insertion and extraction.

According to our previous investigation, a 100% volume variation corresponds to a lithium storage capacity of 1500 mAh g^{-1} [8]. Since the discharge capacity is fixed and corresponds to 4200 mAh g^{-1} , the extra capacity must be contributed from the Si substrate. The nanopillar Si top layer contributes 1500 mAh g^{-1} . Therefore, in the case of the 5 nm Al_2O_3 coated sample B, most of the capacity should be contributed by the substrate layer. The insertion of a large amount of lithium into the Si substrate could lead to the formation of penetration cracks through the Si wafer, as observed in this sample, shown in figure 11, which is not observed in the other samples.

For samples C and D, the results in figures 10(a) and (b) are quite encouraging since the 5 nm Cu-coated nanopillars show a smaller increase of height but a higher total volume variation, due to only having a significant lateral expansion. It means that a 5 nm Cu coating does not block lithium insertion into Si nanopillars. Instead, the Cu coating layer is beneficial to electron transport. Consequently, sample C shows the most significant volume variation, indicating a high lithium storage capacity. The significant anisotropic expansion of sample C is different from previous investigations: in Si microdisks with an aspect ratio of 200 nm height to 8000 nm diameter [7] or 500 nm height to 5000 nm diameter, the expansion occurs mainly in the vertical direction, due to a

two-phase reaction mechanism and interactions between the substrate and the top layer [27]. Our new results agree with SiNWs investigations [15, 16]. In our case, the height is about 600 nm and the average diameter of the Si pillars is about 100 nm.

Sample D shows similar behavior to sample C but with less volume variation at the first cycle. This is reasonable since the increased thickness of the Cu coating layer could also block lithium insertion.

Therefore, the tiny difference in the dQ/dV curves and the increase of the capacity during cycling can be understood, since the main capacities for the 5 nm Al_2O_3 and 10 nm Cu-coated NTSTF electrodes could be contributed from the substrate.

3. Summary

In this work, we have investigated the electrochemical performances and volume variation of nano-textured silicon thin films, both uncoated and coated with 5 nm Al_2O_3 , 5 nm and 10 nm Cu thin films. It is found that the 5 nm Cu coating shows the largest activity for the top layer of the Si nanopillar. This should be related to the enhanced electron transport from the substrate to the top. It is found that the porous structure is not stable during cycling due to electrochemical agglomeration. It seems that the decrease in the porosity has no significant impact on the cyclic performance. Although the top layer Si pillars in the NTSTF electrode show no theoretical capacity due to kinetic issues, the observed significant anisotropic volume variation in this type of cheap material, where the height of the active layer does not change and only the lateral direction expands and contracts, is still very encouraging. The present materials are not practical since a silicon wafer is used; however, further material design could be considered based on this finding. For example, textured amorphous silicon films grown directly on a current collector (i.e. graphene sheet, Cu sheet) could be more promising.

Acknowledgments

Financial support from CAS project KJCX2-YW-W26 is acknowledged. The authors are grateful for help from

Mr Guoqiang Yu and Professor Xiufeng Han of the Institute of Physics at the CAS for Cu dc sputtering.

References

- [1] Dey A N 1971 *J. Electrochem. Soc.* **118** 1547
- [2] Weydanz W J, Wohlfahrt M M and Huggins R J 1999 *J. Power Sources* **81/82** 237
- [3] Li H, Huang X J, Chen L Q, Zhou G, Zhang Z and Yu D 2000 *Solid State Ion.* **135** 181
- [4] Hatchard T D and Dahn J R 2004 *J. Electrochem. Soc.* **151** A838
- [5] Key B, Bhattacharyya R, Morcrette M, Seznec V, Tarascon J M and Grey C P 2009 *J. Am. Chem. Soc.* **131** 9239
- [6] Liu X H, Zhang L Q, Zhong L, Liu Y, Zheng H and Wang J W 2011 *Nano Lett.* **11** 2251
- [7] Beaulieu L Y, Hatchard T D, Bonakdarpour A, Fleischauer M D and Dahn J R 2003 *J. Electrochem. Soc.* **150** A1457
- [8] He Y, Yu X, Li G, Wang R, Li H, Wang Y and Huang X J 2012 *J. Power Sources* **216** 131
- [9] Wang Y H, He Y, Xiao R J, Li H, Aifantis K E and Huang X J 2012 *J. Power Sources* **202** 236–45
- [10] Li H, Huang X J, Chen L Q, Wu Z G and Liang Y 1999 *Electrochem. Solid State Lett.* **11** 547
- [11] Todd A D W, Mar R E and Dahn J R 2007 *J. Electrochem. Soc.* **154** A597
- [12] Yoshio M, Wang H Y, Fukuda K, Umeno T, Dimov N and Ogumi Z 2002 *J. Electrochem. Soc.* **149** A1598
- [13] Lee K T, Jung Y S S and Oh M 2003 *J. Am. Chem. Soc.* **125** 5652
- [14] Li H, Wang Z X, Chen L Q and Huang X J 2009 *Adv. Mater.* **21** 4593
- [15] Liu X H, Zheng H, Zhong L, Huang S, Karki K and Zhang L Q 2011 *Nano Lett.* **11** 3312–8
- [16] Lee S W, McDowell M T, Choi J W and Cui Y 2011 *Nano Lett.* **11** 3034–9
- [17] Wang Y, Schmidt V, Senz S and Gosele U 2006 *Nature Nanotechnol.* **1** 186–9
- [18] Chan C K, Peng H, Liu G, McIlwrath K, Zhang X F and Huggins R A 2008 *Nature Nanotechnol.* **3** 31–5
- [19] Laïk B, Eude L, Pereira-Ramos J P, Cojocar C S, Pribat D and Rouvière E 2008 *Electrochim. Acta* **53** 5528–32
- [20] Gohier A, Laïk B, Pereira-Ramos J-P, Cojocar C S and Tran-Van P 2012 *J. Power Sources* **203** 135–9
- [21] Lin S Y, Fleming J G, Hetherington D L, Smith B K, Kurtz S R and Bur J 1998 *Nature* **394** 251–3
- [22] Tutt L W and Boggess T F 1993 *Prog. Quantum Electron.* **17** 39
- [23] Koynov S, Brandt M S and Stutzmann M 2006 *Appl. Phys. Lett.* **88** 203107
- [24] Yuan H C, Yost V E, Page M R, Stradins P, Meier D L and Branz H M 2009 *Appl. Phys. Lett.* **95** 123501
- [25] Liu Y, Lai T, Li H, Wang Y, Mei Z and Liang H 2012 *Small* **8** 1392–7
- [26] He Y, Yu X, Wang Y, Li H and Huang X J 2011 *Adv. Mater.* **23** 4938–41
- [27] Wang J W et al 2013 *Nano Lett.* **13** 709–15